Deep Learning for XRD Structural Fingerprinting: E3NN Based Atomic Cluster Expansion Contrastive Learning

Xiao Zhang , Xitao Wang , Shunbo Hu *

Posted Date: 23 April 2025

doi: 10.20944/preprints202504.1913.v1

Keywords: Contrastive learning; SE(3)-equivariant graph neural networks; Low-symmetry crystal systems

 doi:10.20944/preprints202504.1913.v1

Article

Deep Learning for XRD Structural Fingerprinting: E3NN Based Atomic Cluster Expansion Contrastive Learning

Xiao Zhang [1,2], Xitao Wang [1,2,3] and Shunbo Hu [1,2,3,*]

[1] Institute for the Conservation of Cultural Heritage, School of Cultural Heritage and Information Management, Shanghai University, Shanghai 200444, China
[2] Key Laboratory of Silicate Cultural Relics Conservation (Ministry of Education), Shanghai University, Shanghai 200444, China
[3] Institute for Quantum Science and Technology and Materials Genome Institute, Shanghai University, Shanghai 200444, China
* Correspondence: shunbohu@shu.edu.cn

Abstract: This study introduces a novel contrastive learning-based X-ray diffraction (XRD) analysis framework, SE(3)-equivariant graph neural networks (E3NN)[1] based Atomic Cluster Expansion Neural Network (EACNN), which reduces the strong dependency on databases and initial models in traditional methods. By integrating E3NN with atomic cluster expansion (ACE) techniques, a dual-tower contrastive learning model has been developed, mapping crystal structures and XRD patterns to a continuous embedding space. The EACNN model retains hierarchical features of crystal systems through symmetry-sensitive encoding mechanisms and utilizes relationship mining via contrastive learning to replace rigid classification boundaries. This approach reveals gradual symmetry-breaking patterns between monoclinic and orthorhombic crystal systems in the latent space, effectively addressing the recognition challenges associated with low-symmetry systems and small sample space groups. Our investigation further explores the potential for model transfer to experimental data and multimodal extensions, laying the theoretical foundation for establishing a universal structure-property mapping relationship.

Keywords: contrastive learning; SE(3)-equivariant graph neural networks; low-symmetry crystal systems

1. Introduction

Since the first discovery of crystal X-ray diffraction by Max von Laue in 1912[2], diffraction patterns have always been a core analytical tool in materials science, serving as the fingerprint of material structures. The Bragg equation $n\lambda = 2d\sin\theta$, proposed by W.H. and W.L. Bragg[3], laid the foundation for diffraction theory, and the invention of the Debye-Scherrer powder diffraction technique[4] made rapid characterization of polycrystalline and amorphous materials possible. With the innovation of synchrotron radiation sources, two-dimensional pixel detectors, and computational methods[5], modern diffraction techniques have evolved from simple lattice constant measurements to multidimensional information probes for analyzing complex structures such as defects, nanodomains, and superlattices. In this development, spectrum analysis and refinement have always been the key bridge connecting experimental data to real structures. Traditional Rietveld refinement methods[6] achieve iterative optimization of structural parameters by minimizing the residual between experimental and theoretical model spectra, but their effectiveness is highly dependent on the accuracy of the initial model, and the computational cost for complex systems (such as mixed phases, low-symmetry materials) grows exponentially. In recent years, the introduction of machine learning techniques[7,8] has brought a paradigm shift to diffraction analysis: by automatically extracting features such as

 doi:10.20944/preprints202504.1913.v1

peak positions, peak widths, and intensity distributions, combined with high-throughput computing, the efficiency of structure analysis has been significantly improved. The bridging role of X-ray diffraction (XRD) technology in this process has become increasingly prominent: experimental XRD patterns are the physical response of real material structures, while simulated XRD patterns of atomic structures provide a golden standard for theoretical verification[9]. Accurate comparison between the two not only verifies the correctness of structural models but also reflects the impact mechanisms of experimental conditions on the data.

Traditional XRD phase identification completes the match by comparing the sample diffraction peak positions, relative intensities, and interplanar spacing with the three core parameters of PDF cards[10]. In the unconditional search mode of the well-known Jade software, even without specifying the chemical composition, it still relies on the "three strong peaks" characteristic data stored in the PDF card database for similarity ranking. For this reason, when a sample contains unknown phases or structures not included in the database, the system cannot generate effective matching results. With the rapid development of new functional materials (such as MOFs, two-dimensional heterojunctions), the growth of existing databases still fails to cover all possible crystal variants[11]. When the diffraction peak positions of unknown structures have a match degree lower than the FOM threshold with existing cards, traditional methods can only classify them as "unknown phases" and cannot conduct in-depth analysis. Even advanced methods like Rietveld refinement face convergence difficulties, attributed to the fact that refinement essentially involves adjusting variables such as the unit cell parameters and atomic coordinates of the initial structure, which heavily depends on known crystal structures as the starting point[6]. This situation highlights the dual paradox of modern XRD analysis: on one hand, phase identification based on PDF card databases remains an important standard for routine laboratory analysis[12]; on the other hand, the inadequate ability to identify substances outside the database has severely constrained the efficiency of new material development.

The introduction of machine learning technology in XRD analysis has provided a revolutionary breakthrough in addressing the strong database dependence and limitations of initial models faced by traditional methods. Machine learning methods differ from manually preset features such as peak positions and intensities (like the "three strongest peaks" rule in PDF cards) by automatically learning higher-order features through the training of convolutional operators or attention mechanisms on spectral information. In recent scientific research, various machine learning algorithms have demonstrated their powerful data-driven processing capabilities[13]. Davel et al.[14] proposed a machine learning framework for materials discovery and characterization using X-ray scattering data. Prasianakis et al.[15] proposed an AI-enhanced framework for real-time mineral phase identification and quantification using X-ray diffraction analysis. Surdu et al.[16] discussed in detail a series of advancements in the application of machine learning in the field of XRD data analysis. Specifically, support vector machines (SVM), convolutional neural networks (CNN), random forests (RF), k-nearest neighbors (KNN), decision trees (DT), gradient boosting, and naive Bayes (NB) have shown advantages in scenarios such as feature extraction from XRD images (e.g., synchrotron radiation data stream analysis[17]), anomaly detection[18], crystal system classification (recognition of seven crystal systems[19,20]), identification of perovskite and non-perovskite materials[21], and classification of geothermal rock minerals[22]. In more microscopic fields, machine learning methods are being widely applied to crystal structure analysis, including cubic lattice structure classification, space group and crystal symmetry prediction, and phase transition analysis. Techniques such as dynamic time warping (DTW), autoencoders, extremely randomized trees (ERT), and deep neural networks (DNN) have shown unique advantages in these tasks. For example, Vecsei et al.[23] proposed a neural network-based method for classifying crystal symmetry from X-ray diffraction patterns, which can effectively identify cubic lattice structures. Similarly, Suzuki et al.[24] achieved successful prediction of crystal space groups and symmetries from X-ray diffraction data using an interpretable machine learning method. These studies indicate that machine learning methods have significant potential in handling

 doi:10.20944/preprints202504.1913.v1

complex crystallographic data. Moreover, Venderley et al.[25] utilized unsupervised machine learning techniques to address the big data processing issues in modern X-ray diffraction data, providing new tools for phase transition analysis. Utimula et al.[26] successfully distinguished the composition of ThMn12-type alloys through machine learning clustering techniques. In terms of feature extraction, autoencoders have been proven to be an effective tool, capable of constructing feature spaces from XRD patterns[27].

In recent years, the paradigm of self-supervised learning, particularly contrastive learning, has seen rapid development in materials science, with its unique multi-modal mutual learning model and strong zero-shot capabilities significantly enhancing the perception of physical information[28]. The combination of contrastive learning with XRD structural analysis has made it possible to break through the paradigm from "hard classification" to "exploration of the correlation between structural and spectroscopic information." In this task scenario, common direct classifier models map simulated spectra to discrete crystal system/space group labels, which is essentially a lossy compression. While it is easy to train, it loses the complex physical correlations between spectra and structures, such as atomic arrangement symmetry and Bragg condition response patterns[29,30]. Contrastive learning, on the other hand, builds a joint embedding space for structure and spectra, directly modeling the potential correspondence between the two, thereby preserving multi-dimensional physical features. In fact, spectra and structures inherently have a one-to-many ambiguity (such as the XRD spectra of four different structural models being highly similar, as mentioned in[31]). The same spectrum may come from different samples, and since the spectrum itself is a statistical representation after dimensionality reduction and averaging, solving this ambiguity from the perspective of the spectrum alone is very challenging[31]. However, the training of contrastive learning is bidirectional: on one hand, the model needs to learn the deterministic generation pattern of the spectrum corresponding to the current structure; on the other hand, it also needs to learn the probabilistic inverse mapping constraint of the structure corresponding to the spectrum. This physically consistent learning method of crystal-pair diffraction spectra is more intrinsic compared to just classifying spectra. Contrastive learning only requires weak supervision signals such as "spectrum A' of structure A should be similar to other augmented versions of structure A (such as rotations, noise perturbations) but different from the spectrum of structure B"[30,32]. This characteristic allows for the use of unlabeled experimental data to enhance training. Therefore, when facing the challenge of "long-tail distribution" (displaying a figure of a category with fewer space groups), simple direct classification of spectra will fail due to the lack of samples for rare space groups, whereas contrastive learning, by emphasizing relationships between samples rather than absolute categories, can utilize a small number of samples to establish boundaries of difference with common categories. This paradigm shift essentially redefines the mathematical formulation of the "structure-spectrum" mapping problem: from a closed category space discrimination to an open relationship manifold learning, resulting in a continuous diffraction spectrum-crystal fingerprint. In the continuous embedding space, crystal symmetry breaking is represented as a gradual change in the curvature of the manifold, rather than a discrete category jump[30,32].

In our work, inspired by the Contrastive Language-Image Pre-training (CLIP) model[33], we integrated SE(3)-equivariant[1] network architecture and atomic cluster expansion (ACE)[34,35] technology to construct a dual-tower contrastive learning model: E3NN-based Atomic Cluster Expansion Neural Network (EACNN). As illustrated in Figure 1 ,crystal structures are processed through a structure encoding tower based on graph neural networks, which interacts with spectral information processed through a 1D ResNet structure for information aggregation in the hidden layer. In our tests, the TOP-1, TOP-3, and TOP-5 accuracies for retrieving structures from XRD spectra were 95.96%, 99.95%, and 99.98% respectively. Moreover, even in samples with very few space group instances, our model maintains robust performance. The remainder of this paper is organized as follows: Section 2 introduces the EACNN framework, detailing its SE(3)-equivariant graph neural network architecture

 doi:10.20944/preprints202504.1913.v1

combined with atomic cluster expansion for crystal structure and XRD pattern encoding. Section 3 demonstrates the model's effectiveness in structure retrieval, particularly in handling symmetry variations and rare space groups. Section 4 concludes by highlighting the method's potential for XRD analysis while addressing current limitations and future directions, including experimental data adaptation and multimodal extension.

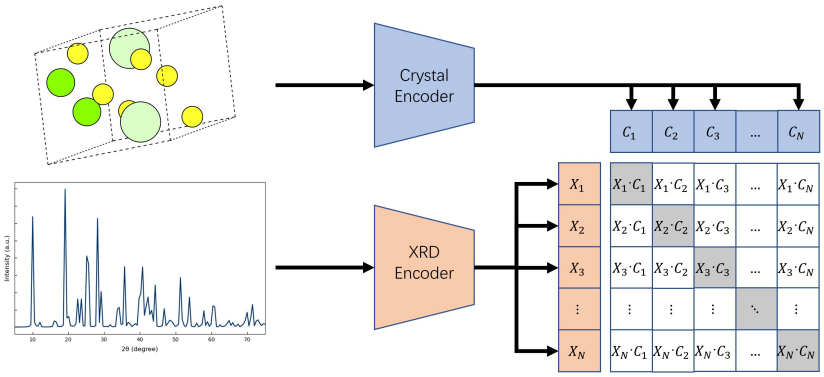

Figure 1. Schematic diagram of the model architecture

2. Materials and Method

2.1. Calculation of the Simulated Spectrum

For any input crystal, after entering the cell parameters $(a, b, c, \alpha, \beta, \gamma)$, space group number, and atomic coordinates occupancy, the equivalent atomic coordinates are automatically generated through Wyckoff position analysis to ensure compliance with space group symmetry. All possible crystal face indices (hkl) are traversed, and the corresponding diffraction angle θ is calculated according to Bragg's equation $n\lambda = 2d_{hkl} \sin\theta$, where the interplanar spacing d_{hkl} is directly calculated from the cell parameters and crystal face indices. Based on the atomic scattering factor f_j and Debye-Waller factor B_j, the structure factor for each (hkl) plane is calculated:

$$F_{hkl} = \sum_j f_j e^{-B_j(\sin\theta/\lambda)^2} e^{2\pi i(hx_j + ky_j + lz_j)} \tag{1}$$

Efficiency can be improved by calculating only the independent reflections through symmetry reduction, as described in Fredericks et al.[36]. The squared modulus of the structure factor $|F_{hkl}|^2$ is multiplied by the Lorentz-polarization factor, and the instrumental broadening function (such as a Gaussian/Lorentzian mixed peak shape) is overlaid to obtain the continuous diffraction spectrum.

2.2. Datasource

All crystal structures come from the Materials Project database, which includes a total of 154,714 samples distributed across 228 space groups. The frequency distribution of the space group numbers of the samples is shown in Figure 2.

 doi:10.20944/preprints202504.1913.v1

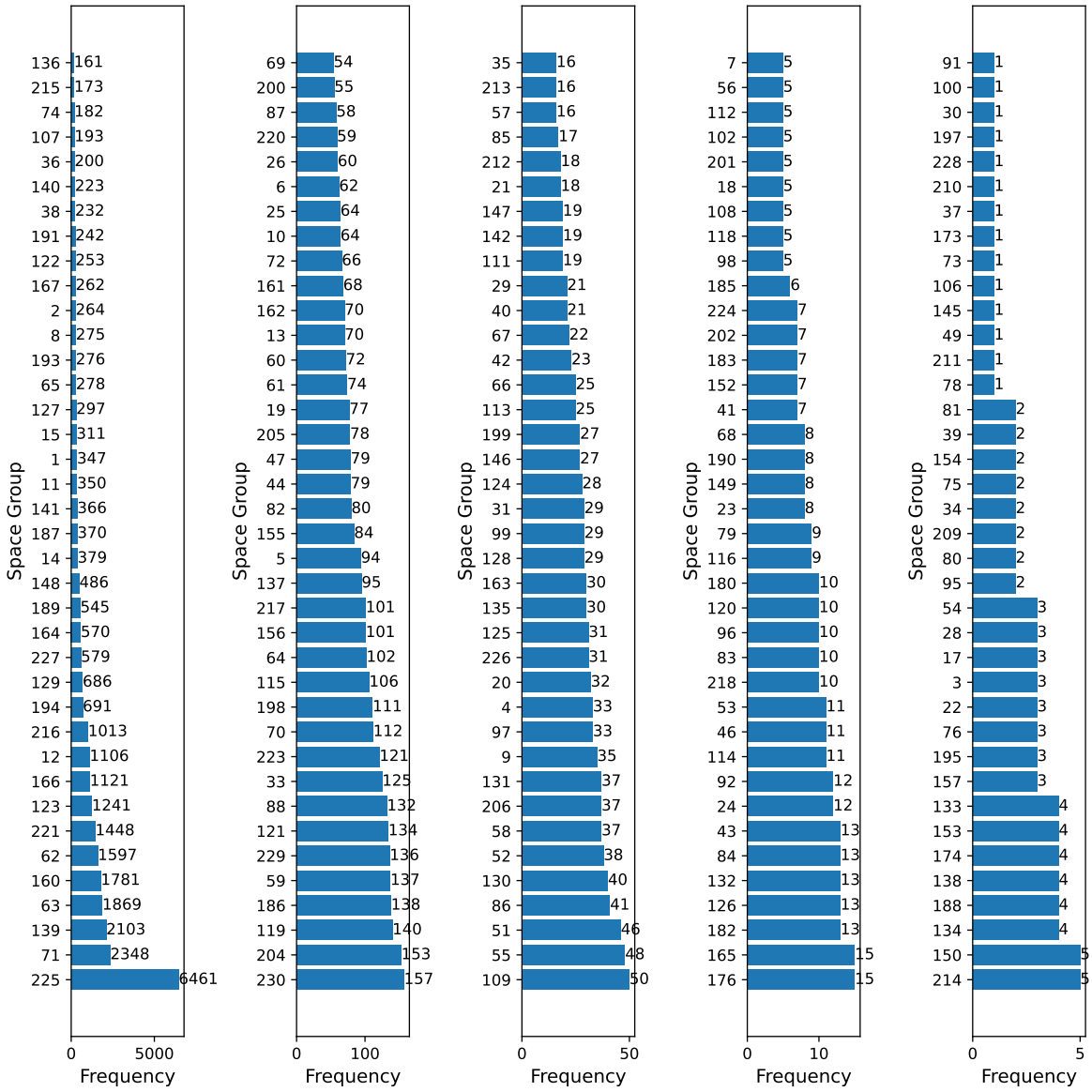

Figure 2. Frequency distribution chart of each space group

In traditional classification models, direct classification of space groups may be challenging due to the imbalance of samples, leading to coupling bias in the symmetry hierarchy and feature distribution. For example, high-symmetry space groups of the cubic crystal system (such as $Fm\bar{3}m$) are significantly more prevalent in the MP database than low-symmetry space groups (such as $P1$ of the triclinic crystal system). This long-tail distribution can cause the model to tend to classify ambiguous samples into high-symmetry categories. More seriously, the symmetry-breaking paths of different crystal systems are non-uniformly separable in the feature space—decision boundaries of high-symmetry crystal systems often dominate, while the fine-grained features of low-symmetry crystal systems are easily overwhelmed by the mainstream distribution in the high-dimensional manifold. Classifiers based on handcrafted features (such as cell parameters and space group numbers) cannot decouple lattice symmetry from atomic primitive features. For example, the monoclinic $P2_1/c$ and the orthorhombic $Pbam$ may overlap in cell parameters and some diffraction peak positions, but they differ fundamentally in microsymmetry features such as screw axes and glide planes. The hard classification boundaries of traditional models can blur the gradual features of such symmetry breaking.

 doi:10.20944/preprints202504.1913.v1

2.3. Crystal Structure Encoder

This work decouples the multiscale features of more than 10^5 crystal structures in the MP database using a deep neural network, preserving the sensitivity of cluster expansion to short-range order while further integrating dynamic correlation patterns across lattices.

$$E_i(\sigma) = \sum_{K,\mathbf{n},\mathbf{l}} c^{(K)}_{\mathbf{n},\mathbf{l}} B^{(K)}_{i,\mathbf{n},\mathbf{l}} \tag{2}$$

In eq.2, K represents the order of the cluster, n and $\mathbf{l}$ represent the indices of the radial and angular basis functions, respectively, $B^{(K)}_{i,\mathbf{n},\mathbf{l}}$ are rotationally invariant basis functions constructed from the product of reduced spherical harmonics, and $c^{(K)}_{\mathbf{n},\mathbf{l}}$ are the undetermined expansion coefficients.

Through network methods, this work follows the theoretical framework of MACE[35], which combines atomic cluster expansion with the multi-body interaction network framework of MPNN(Message Passing Neural Networks[37]), forming an equivariant encoder for encoding crystal structures.

At the primary feature layer, the convolutional module captures geometric features closely related to the cluster expansion parameters, such as atomic distances and coordination numbers; at the advanced semantic layer, the graph neural network dynamically models the long-range correlation effects between clusters through message passing, breaking the limitation of fixed cutoff radii in traditional cluster expansions.

$$m_i^{(t)} = \sum_j u_1\left(\sigma_i^{(t)}; \sigma_j^{(t)}\right) + \sum_{j_1,j_2} u_2\left(\sigma_i^{(t)}; \sigma_{j_1}^{(t)}, \sigma_{j_2}^{(t)}\right) + \cdots + \sum_{j_1,\ldots,j_\nu} u_\nu\left(\sigma_i^{(t)}; \sigma_{j_1}^{(t)}, \ldots, \sigma_{j_\nu}^{(t)}\right) \tag{3}$$

where in eq.3,u is learnable, and ν represents the maximum correlation order in the state.

2.4. Diffraction Pattern Encoder

This work inputs the diffraction pattern as a one-dimensional vector of length 140 into the model, aggregates the information into a 384-channel one-dimensional vector through two layers of 1D-resnet[38], and uses this vector as the embedding vector of the diffraction pattern.

The core advantage of 1D convolutional networks in XRD pattern encoding stems from their deep alignment with the characteristics of diffraction signals. As a one-dimensional sequence of angle-intensity, the key information in XRD patterns is embedded in the local peak shape structures: 1D-CNN can accurately capture the position, intensity, and half-width of diffraction peaks through the local perception characteristics of convolutional kernels. Hierarchical convolutional structures can abstract peak shape combination patterns step by step, achieving efficient mapping from atomic-level diffraction features to macroscopic phase recognition.

2.5. Loss Function

The loss function design in this work follows the InfoNCE Loss design from SimCLR[39], using all sample pairs within a batch except for the self-sample pair as negative samples. However, as a multimodal contrastive learning task, this work adopts the mean of the mutual InfoNCE Loss between the two modalities as the final loss of the model, a form consistent with the final Loss design of CLIP[33]:

$$\mathcal{L}_{\text{SimCLR}} = -\frac{1}{2N}\sum_{i=1}^{2N} \log \frac{\exp\left(\frac{z_i^\top z_j}{\tau \|z_i\| \|z_j\|}\right)}{\sum_{k=1}^{2N} 1_{k\neq i} \exp\left(\frac{z_i^\top z_k}{\tau \|z_i\| \|z_k\|}\right)} \tag{4}$$

 doi:10.20944/preprints202504.1913.v1

where in eq.4 , z_i, z_j are feature vectors of the same original sample after different data augmentations; τ is the temperature parameter; N is the batch size, and $1_{k \neq i}$ is a flag to exclude self-comparison.

$$\mathcal{L}_{\text{EACNN}} = \frac{1}{2}\left(\mathcal{L}_{\text{crystal}\to\text{xrd}} + \mathcal{L}_{\text{xrd}\to\text{crystal}}\right) \tag{5}$$

$$\mathcal{L}_{\text{crystal}\to\text{xrd}} = -\frac{1}{B}\sum_{i=1}^{B}\log\frac{\exp\left(\frac{C_i^\top X_i}{\lambda\|C_i\|\|X_i\|}\right)}{\sum_{j=1}^{B}\exp\left(\frac{C_i^\top X_j}{\lambda\|C_i\|\|X_j\|}\right)} \tag{6}$$

$$\mathcal{L}_{\text{xrd}\to\text{crystal}} = -\frac{1}{B}\sum_{i=1}^{B}\log\frac{\exp\left(\frac{X_i^\top C_i}{\lambda\|X_i\|\|C_i\|}\right)}{\sum_{j=1}^{B}\exp\left(\frac{X_i^\top C_j}{\lambda\|X_i\|\|C_j\|}\right)} \tag{7}$$

where in eq.6 and eq.7 , C_i, X_i are the i-th crystal structure and xrd pattern embeddings in the batch, λ is a trainable temperature parameter initially set to 0.07, and B is the batch size.

3. Results and Discussion

EACNN trained on a dataset based on the MP database and tested its performance in reconstructing structures from spectra on an independent test set. For contrastive learning, top-N is commonly used to characterize its performance. The specific Top-N values are presented in Table 1, with the accuracy rates for top-1, top-3, and top-5 being 95.96%, 99.95%, and 99.98%, respectively, even though these matches are entirely based on the model's automatic learning rather than special annotations. From the Table 1, it is evident that the model's performance nearly converges at Top-3.

Table 1. Performance comparison of structure retrieval from XRD spectra

Model	Top-1 (%)	Top-3 (%)	Top-5 (%)
Model Name	95.96	99.95	99.98

From the perspective of feature learning, high top-N accuracy indicates that the model has successfully established a robust mapping in the latent space. Through adversarial training of positive and negative samples in contrastive learning, the model can effectively capture the nonlinear correspondence between atomic arrangements in crystal structures and X-ray diffraction patterns. Further analysis involves the ranking of crystals corresponding to similar spectra in the test set, primarily to observe the similarities and differences between the paired crystals of the detected spectra. As shown in Figure 3, the detected spectra are labeled as True XRD, and the first structure inferred in reverse is the true structure. The model is then required to infer the second structure (most similar structure) and simultaneously extract its corresponding XRD. The model is further instructed to output the third inference structure, and the same method is used to extract the second similar structure and its corresponding XRD.

From the model's inference results shown in Figure 3, the space group of the crystal structure corresponding to the detected XRD is $P2_1/c$ (monoclinic, Bravais lattice type P). The space group of the Top-2 inferred structure is Pbam (orthorhombic, Bravais lattice type P), and the space group of the Top-3 inferred structure has extended to $C2/m$ (monoclinic, Bravais lattice type C). Analyzing from the perspective of symmetry evolution, the model's prediction ranking of $P2_1/c$, $Pbam$, and $C2/m$ reveals a deep connection between the hierarchy of symmetry breaking and diffraction characteristics, despite the significant overlap of XRD patterns in specific angular ranges, as shown by the strong peak clusters. This symmetry-sensitive prediction mechanism may originate from E(3) invariance and strong local learning constraints in cluster expansion: 1. During data augmentation, by applying

 doi:10.20944/preprints202504.1913.v1

symmetry transformations allowed by specific space groups (such as glide plane reflections, screw axis translations) to atomic positions, the invariance constraint under symmetry operations forces the model to learn intrinsic symmetry features rather than being limited to specific atomic coordinate arrangements. For example, the screw axis operation of $P2_1/c$ generates a periodic phase shift in the diffraction intensity distribution, and the model filters out such non-essential differences through an invariance loss function. 2. Lattice symmetry components (related to Bravais types) and atomic primitive components (related to Wyckoff positions) are automatically learned and undergo distance relaxation during the aggregation of local representations (the essence of contrastive learning is to re-adjust the distances between samples), such as the significant separation of $P2_1/c$ and $C2/m$ in the lattice symmetry subspace (Bravais types are explicitly separated), but they are similar in the atomic primitive subspace. This differs fundamentally from traditional database queries, which typically rely on preset structural descriptors (such as space group numbers, cell parameter thresholds) or empirical peak position similarity (such as Euclidean distance), and cannot distinguish between symmetry breaking due to differences in Bravais lattice types (such as P→C) and pseudo-symmetry caused by atomic primitive perturbations. Additionally, the deep learning method also compensates for the lack of local-global feature coupling, as traditional methods usually handle lattice parameters and atomic positions independently, while deep models can achieve multi-scale aggregation, establishing dynamic associations between local chemical environment features in cluster expansion and global symmetry features.

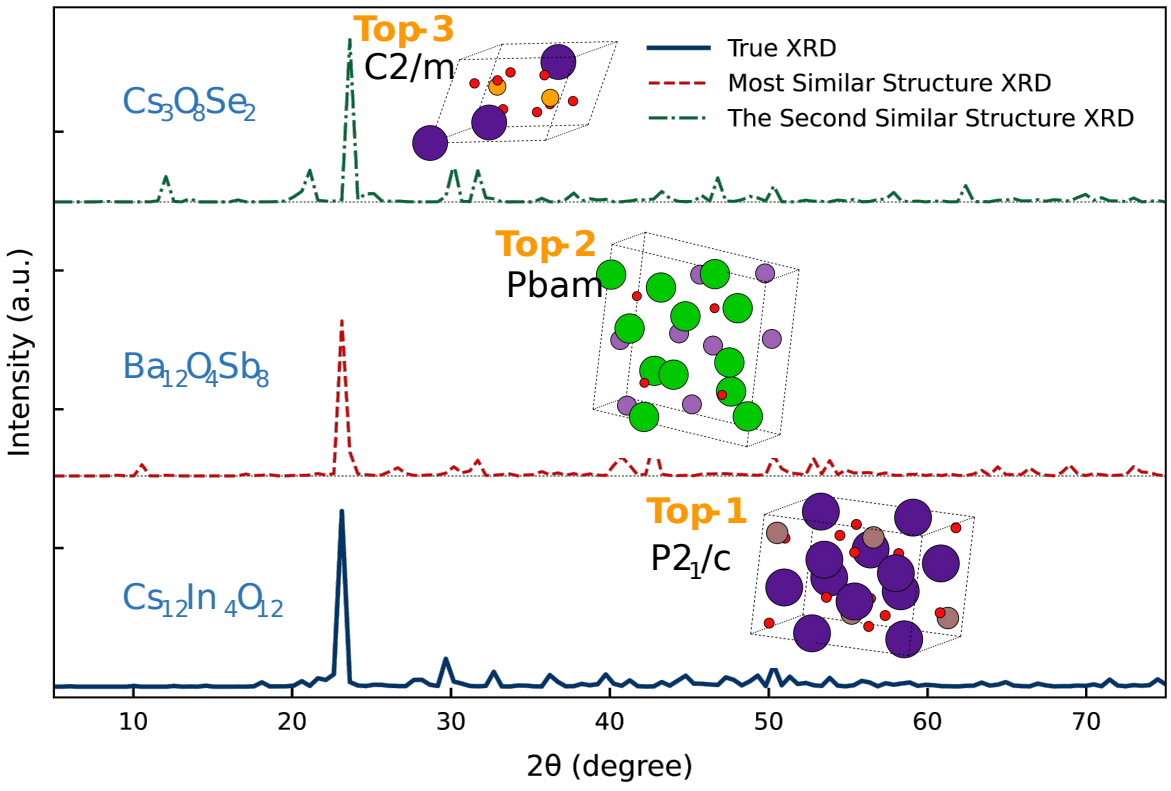

Figure 3. Structural Inference from True XRD and the Inferred Structures' Diffraction Patterns

To further analyze the physical information learned by the model, t-SNE[40] was used to reduce the dimensionality and visualize the hidden layer of the model. From Figure 4, it can be seen that while some local clustering effects of crystal systems are retained during contrastive learning training, the overall clustering is not significantly constrained by crystal systems.

 doi:10.20944/preprints202504.1913.v1

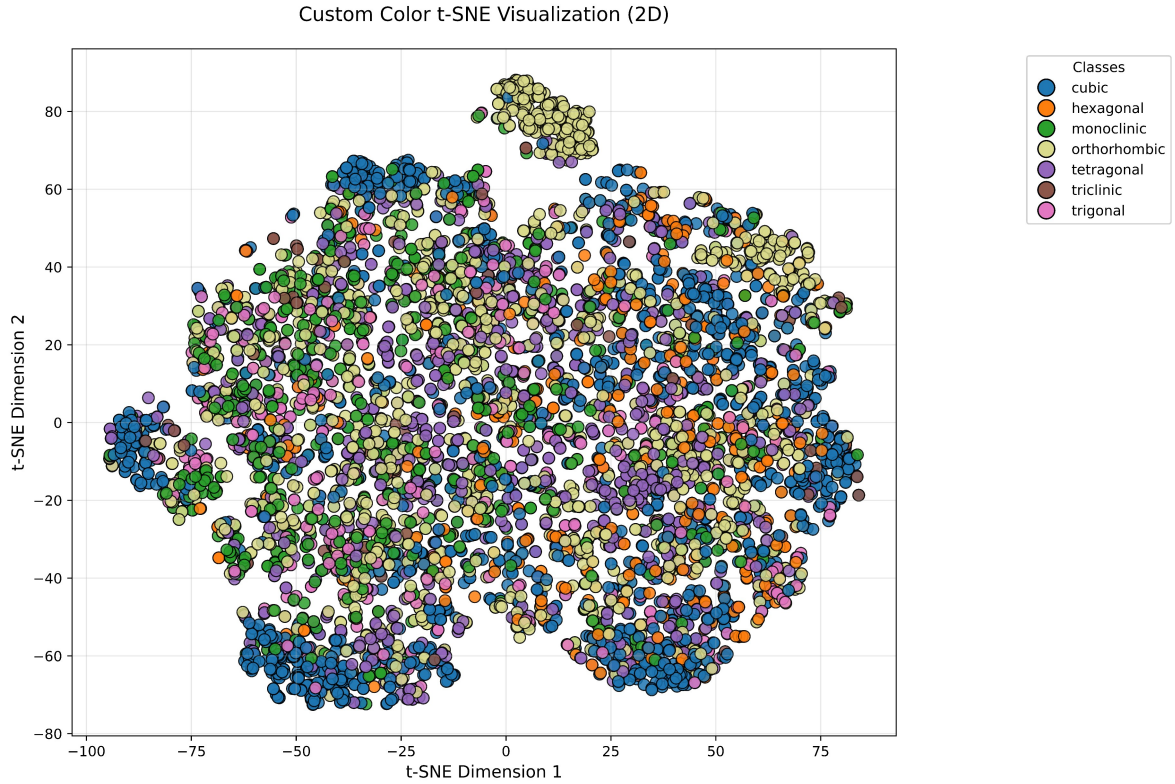

Figure 4. Visualization of hidden layers in contrastive learning vs seven crystal systems

In traditional methods, the feature distributions of the seven crystal systems exhibit discrete hard boundaries (such as the sharp division between cubic and hexagonal systems), which stem from the linear dependence of handcrafted features on cell parameters (such as the strong constraint of $a = b = c$ in cubic systems). Through the soft clustering mechanism of contrastive learning, high-symmetry crystal systems (such as cubic) still maintain local clustering, indicating that the features of high-symmetry crystal systems still have strong distinguishability in the model's latent space, while low-symmetry crystal systems (monoclinic, triclinic) form a gradual transition zone. For example, the distribution of potential vectors for monoclinic and orthorhombic systems partially overlaps, as the lower symmetry of monoclinic and triclinic systems results in a larger range of variations in cell parameters and atomic arrangements, making them susceptible to lattice distortions and leading to the blurring of feature distributions.

Due to this personalized recognition approach, contrastive learning is not limited by the influence of strict hard classification categories. We randomly selected some space group samples with small sample sizes and samples of the space group $Fm\bar{3}m$ with a large number of test samples to test the space group accuracy after top1 recognition, as shown in Table 2.

Table 2. Space group frequency and accuracy. Tables should be placed in the main text near to the first time they are cited.

Space Group	Frequency	Accuracy
225	808	95.92%
3, 24, 34, 37, 39 41, 48, 50, 95, 97 112, 116, 120, 132, 138 143, 157, 159, 180, 192 195, 197, 202, 203, 214	1 (each)	96.00%

 doi:10.20944/preprints202504.1913.v1

From Table 2, it can be seen that the individual characteristics of small samples are well preserved. The complementary nature of cluster expansion with E3 invariance and contrastive training in the feature space provides a dual guarantee for model performance improvement: the former ensures feature interpretability through a clear physical parameterization process, while the latter mines implicit cross-scale correlation patterns through a data-driven approach. This hybrid paradigm not only retains prior knowledge in the field of materials science but also fully leverages the nonlinear fitting advantages of deep learning, providing new insights for establishing a universal structure-property mapping relationship.

4. Conclusions

The integration of contrastive learning with crystallographic analysis represents a paradigm shift in XRD-based material characterization. Our model achieves remarkable Top-1 (95.96%), Top-3 (99.95%), and Top-5 (99.98%) accuracies in structure retrieval tasks, significantly outperforming traditional database-matching methods constrained by predefined PDF card features. By redefining XRD analysis as a continuous manifold learning problem, our contrastive learning framework transcends the limitations of conventional classification paradigms. It not only advances structure identification for database-excluded materials but also provides a foundation for autonomous materials discovery systems. The synergy between equivariant neural networks and physics-driven constraints opens new avenues for decoding complex structure-property relationships across materials science.

While our approach excels in simulated XRD data, experimental complexities—such as preferred orientation effects, instrumental broadening, and amorphous background signals—require further adaptation. Future work should incorporate domain adaptation techniques to align simulated and experimental feature distributions. Additionally, extending the framework to multimodal data (e.g., pairing XRD with PDF analysis or spectroscopy) could enhance structural resolution for disordered systems. The current model's reliance on Materials Project data also necessitates validation against experimentally synthesized novel materials, particularly metastable phases absent in computational databases.

Author Contributions: Conceptualization, X.Z. and S.H.; Methodology, X.W. and S.H.; Validation, X.Z. and X.W.; Formal analysis, X.W.; Investigation, X.Z.; Resources, S.H.; Data curation, X.Z.; Writing—original draft preparation, X.Z.; Writing—review and editing, S.H.; Visualization, X.W.; Supervision, S.H.; Project administration, S.H.; Funding acquisition, S.H. All authors have read and agreed to the published version of the manuscript.

Funding: This research was funded by the National Key R&D Program of China (Grant No. 2023YFB4402600), the National Natural Science Foundation of China (Grant Nos. 52271007, 12074241, 22173058, 12274278, 12274279), the Major Science and Technology Projects of Shanxi Province (No. 202201150501024), and the Shanghai Technical Service Center of Science and Engineering Computing, Shanghai University. The APC was funded by the National Natural Science Foundation of China (Grant No. 52271007).

Institutional Review Board Statement: Not applicable.

Informed Consent Statement: Not applicable.

Data Availability Statement: The datasets used and analyzed during the current study are available from the corresponding author upon reasonable request.

Conflicts of Interest: The authors declare no conflicts of interest.

 doi:10.20944/preprints202504.1913.v1

References

1. Du, W.; Zhang, H.; Du, Y.; Meng, Q.; Chen, W.; Zheng, N.; Shao, B.; Liu, T.Y. SE (3) equivariant graph neural networks with complete local frames. In Proceedings of the International Conference on Machine Learning. PMLR, 2022, pp. 5583–5608.
2. Friedrich, W.; Knipping, P.; Laue, M. Interferenzerscheinungen bei roentgenstrahlen. *Annalen der Physik* **1913**, *346*, 971–988.
3. Bragg, W.H.; Bragg, W.L. The reflection of X-rays by crystals. *Proceedings of the Royal Society of London. Series A, Containing Papers of a Mathematical and Physical Character* **1913**, *88*, 428–438.
4. Debye, P.; Scherrer, P. Interferenzen an regellos orientierten Teilchen im Röntgenlicht. I. *Nachrichten von der Gesellschaft der Wissenschaften zu Göttingen, Mathematisch-Physikalische Klasse* **1916**, *1916*, 1–15.
5. Toby, B.H.; Von Dreele, R.B. GSAS-II: the genesis of a modern open-source all purpose crystallography software package. *Applied Crystallography* **2013**, *46*, 544–549.
6. Rietveld, H.M. A profile refinement method for nuclear and magnetic structures. *Applied Crystallography* **1969**, *2*, 65–71.
7. Park, W.B.; Chung, J.; Jung, J.; Sohn, K.; Singh, S.P.; Pyo, M.; Shin, N.; Sohn, K.S. Classification of crystal structure using a convolutional neural network. *IUCrJ* **2017**, *4*, 486–494.
8. Oviedo, F.; Ren, Z.; Sun, S.; Settens, C.; Liu, Z.; Hartono, N.T.P.; Ramasamy, S.; DeCost, B.L.; Tian, S.I.; Romano, G.; et al. Fast and interpretable classification of small X-ray diffraction datasets using data augmentation and deep neural networks. *npj Computational Materials* **2019**, *5*, 60.
9. Billinge, S.J.; Levin, I. The problem with determining atomic structure at the nanoscale. *science* **2007**, *316*, 561–565.
10. Jenkins, R.; Snyder, R.L.; et al. *Introduction to X-ray powder diffractometry*; Vol. 138, Wiley Online Library, 1996.
11. Furukawa, H.; Cordova, K.E.; O'Keeffe, M.; Yaghi, O.M. The chemistry and applications of metal-organic frameworks. *Science* **2013**, *341*, 1230444.
12. O'keeffe, M.; Peskov, M.A.; Ramsden, S.J.; Yaghi, O.M. The reticular chemistry structure resource (RCSR) database of, and symbols for, crystal nets. *Accounts of chemical research* **2008**, *41*, 1782–1789.
13. Su, T.; Cao, B.; Hu, S.; Li, M.; Zhang, T.Y. CGWGAN: crystal generative framework based on Wyckoff generative adversarial network. *Journal of Materials Informatics* **2024**, *4*, N–A.
14. Davel, C.; Bassiri-Gharb, N.; Correa-Baena, J.P. Machine Learning in X-ray Scattering for Materials Discovery and Characterization **2024**.
15. Prasianakis, N.I. AI-enhanced X-ray diffraction analysis: towards real-time mineral phase identification and quantification. *IUCrJ* **2024**, *11*, 647–648.
16. Surdu, V.A.; Győrgy, R. X-ray diffraction data analysis by machine learning methods—a review. *Applied Sciences* **2023**, *13*, 9992.
17. Wang, B.; Guan, Z.; Yao, S.; Qin, H.; Nguyen, M.H.; Yager, K.; Yu, D. Deep learning for analysing synchrotron data streams. In Proceedings of the 2016 New York Scientific Data Summit (NYSDS). IEEE, 2016, pp. 1–5.
18. Czyzewski, A.; Krawiec, F.; Brzezinski, D.; Porebski, P.J.; Minor, W. Detecting anomalies in X-ray diffraction images using convolutional neural networks. *Expert systems with applications* **2021**, *174*, 114740.
19. Chakraborty, A.; Sharma, R. See deeper: Identifying crystal structure from x-ray diffraction patterns. In Proceedings of the 2020 International Conference on Cyberworlds (CW). IEEE, 2020, pp. 49–54.
20. Chakraborty, A.; Sharma, R. A deep crystal structure identification system for X-ray diffraction patterns. *The Visual Computer* **2022**, *38*, 1275–1282.
21. Massuyeau, F.; Broux, T.; Coulet, F.; Demessence, A.; Mesbah, A.; Gautier, R. Perovskite or Not Perovskite? A Deep-Learning Approach to Automatically Identify New Hybrid Perovskites from X-ray Diffraction Patterns. *Advanced Materials* **2022**, *34*, 2203879.
22. Ishitsuka, K.; Ojima, H.; Mogi, T.; Kajiwara, T.; Sugimoto, T.; Asanuma, H. Characterization of hydrothermal alteration along geothermal wells using unsupervised machine-learning analysis of X-ray powder diffraction data. *Earth Science Informatics* **2022**, pp. 1–15.
23. Vecsei, P.M.; Choo, K.; Chang, J.; Neupert, T. Neural network based classification of crystal symmetries from x-ray diffraction patterns. *Physical Review B* **2019**, *99*, 245120.
24. Suzuki, Y.; Hino, H.; Hawai, T.; Saito, K.; Kotsugi, M.; Ono, K. Symmetry prediction and knowledge discovery from X-ray diffraction patterns using an interpretable machine learning approach. *Scientific reports* **2020**, *10*, 21790.

 doi:10.20944/preprints202504.1913.v1

25. Venderley, J.; Mallayya, K.; Matty, M.; Krogstad, M.; Ruff, J.; Pleiss, G.; Kishore, V.; Mandrus, D.; Phelan, D.; Poudel, L.; et al. Harnessing interpretable and unsupervised machine learning to address big data from modern X-ray diffraction. *Proceedings of the National Academy of Sciences* **2022**, *119*, e2109665119.
26. Utimula, K.; Hunkao, R.; Yano, M.; Kimoto, H.; Hongo, K.; Kawaguchi, S.; Suwanna, S.; Maezono, R. Machine-Learning Clustering Technique Applied to Powder X-Ray Diffraction Patterns to Distinguish Compositions of ThMn12-Type Alloys. *Advanced Theory and Simulations* **2020**, *3*, 2000039.
27. Utimula, K.; Yano, M.; Kimoto, H.; Hongo, K.; Nakano, K.; Maezono, R. Feature space of XRD patterns constructed by an autoencoder. *Advanced Theory and Simulations* **2023**, *6*, 2200613.
28. Wu, Y.; Su, T.; Du, B.; Hu, S.; Xiong, J.; Pan, D. Kolmogorov–Arnold Network Made Learning Physics Laws Simple. *The Journal of Physical Chemistry Letters* **2024**, *15*, 12393–12400.
29. Lai, Q.; Xu, F.; Yao, L.; Gao, Z.; Liu, S.; Wang, H.; Lu, S.; He, D.; Wang, L.; Zhang, L.; et al. End-to-End Crystal Structure Prediction from Powder X-Ray Diffraction. *Advanced Science* **2025**, *12*, 2410722.
30. Guo, G.; Goldfeder, J.; Lan, L.; Ray, A.; Yang, A.H.; Chen, B.; Billinge, S.J.L.; Lipson, H. Towards end-to-end structure determination from x-ray diffraction data using deep learning. *npj Computational Materials* **2024**, *10*, 209.
31. Schlesinger, C.; Fitterer, A.; Buchsbaum, C.; Habermehl, S.; Chierotti, M.R.; Nervi, C.; Schmidt, M.U. Ambiguous structure determination from powder data: four different structural models of 4, 11-difluoroquinacridone with similar X-ray powder patterns, fit to the PDF, SSNMR and DFT-D. *IUCrJ* **2022**, *9*, 406–424.
32. Parackal, A.S.; Goodall, R.E.; Faber, F.A.; Armiento, R. Identifying crystal structures beyond known prototypes from x-ray powder diffraction spectra. *Physical Review Materials* **2024**, *8*, 103801.
33. Radford, A.; Kim, J.W.; Hallacy, C.; Ramesh, A.; Goh, G.; Agarwal, S.; Sastry, G.; Askell, A.; Mishkin, P.; Clark, J.; et al. Learning transferable visual models from natural language supervision. In Proceedings of the International conference on machine learning. PmLR, 2021, pp. 8748–8763.
34. Drautz, R. Atomic cluster expansion for accurate and transferable interatomic potentials. *Physical Review B* **2019**, *99*, 014104.
35. Batatia, I.; Kovacs, D.P.; Simm, G.; Ortner, C.; Csányi, G. MACE: Higher order equivariant message passing neural networks for fast and accurate force fields. *Advances in neural information processing systems* **2022**, *35*, 11423–11436.
36. Fredericks, S.; Parrish, K.; Sayre, D.; Zhu, Q. PyXtal: A Python library for crystal structure generation and symmetry analysis. *Computer Physics Communications* **2021**, *261*, 107810.
37. Gilmer, J.; Schoenholz, S.S.; Riley, P.F.; Vinyals, O.; Dahl, G.E. Neural message passing for quantum chemistry. In Proceedings of the International conference on machine learning. PMLR, 2017, pp. 1263–1272.
38. He, K.; Zhang, X.; Ren, S.; Sun, J. Deep residual learning for image recognition. In Proceedings of the Proceedings of the IEEE conference on computer vision and pattern recognition, 2016, pp. 770–778.
39. Chen, T.; Kornblith, S.; Norouzi, M.; Hinton, G. A simple framework for contrastive learning of visual representations. In Proceedings of the International conference on machine learning. PmLR, 2020, pp. 1597–1607.
40. Su, T.; Cui, Y.; Lian, Z.; Hu, M.; Li, M.; Lu, W.; Ren, W. Physics-Based Feature Makes Machine Learning Cognizing Crystal Properties Simple. *The Journal of Physical Chemistry Letters* **2021**, *12*, 8521–8527.